World Journal of Gastroenterology

Submit a Manuscript: http://www.f6publishing.com

World J Gastroenterol 2018 January 14; 24(2): 195-210

DOI: 10.3748/wjg.v24.i2.195

ISSN 1007-9327 (print) ISSN 2219-2840 (online)

ORIGINAL ARTICLE

Basic Study

INT-767 improves histopathological features in a diet-induced *ob/ob* mouse model of biopsy-confirmed non-alcoholic steatohepatitis

Jonathan D Roth, Michael Feigh, Sanne S Veidal, Louise KD Fensholdt, Kristoffer T Rigbolt, Henrik H Hansen, Li C Chen, Mathieu Petitjean, Weslyn Friley, Niels Vrang, Jacob Jelsing, Mark Young

Jonathan D Roth, Mark Young, Intercept Pharmaceuticals, Intercept Pharmaceuticals, San Diego, CA 92121, United States

Michael Feigh, Sanne S Veidal, Louise KD Fensholdt, Kristoffer T Rigbolt, Henrik H Hansen, Niels Vrang, Jacob Jelsing, Gubra, Hoersholm DK-2970, Denmark

Li C Chen, Mathieu Petitjean, PharmaNest, Genesis Imaging Services, Princeton, NJ 08540, United States

Weslyn Friley, Qualyst Transporter Solutions, Durham, NC 27713, United States

ORCID number: Jonathan D Roth (0000-0002-8804-8193); Michael Feigh (0000-0001-5274-8799); Sanne S Veidal (0000-0003-1240-2034); Louise KD Fensholdt (0000-0002-9762-3903); Kristoffer T Rigbolt (000 0-0002-9470-0993); Henrik H Hansen (0000-0002-3732-0281); Li C Chen (0000-0002-3458-1830); Mathieu Petitjean (0000-00 03-3468-7114); Weslyn Friley (0000-0002-6992-8726); Niels Vrang (0000-0002-7203-9532); Jacob Jelsing (0000-0 002-4583-1022); Mark Young (0000-0002-9503-6211).

Author contributions: Studies were designed by Roth JD, Feigh M, Petitjean M and Young M; Fensholdt LKD Fensholdt, Veidal SS, Rigbolt KT, Chen LC and Friley W performed the majority of experiments; Hansen HH and Roth JD wrote the paper with significant contributions to data analyses and editing by all co-authors.

Institutional animal care and use committee statement: All animal experiments conformed to the internationally accepted principles for the care and use of laboratory animals (licence no. 2013-15-2934-00784, The Animal Experiments Inspectorate, Denmark).

Conflict-of-interest statement: Jonathan Roth and Mark Young are employed by and hold equity in Intercept Pharmaceuticals, Inc. All other authors have nothing to disclose.

Data sharing statement: No additional data are available.

Manuscript source: Invited manuscript

Correspondence to: Henrik H Hansen, PhD, Principal Scientist, Pharmacology, Gubra, Kongevej 11B, Hoersholm DK-2970, Denmark. hbh@gubra.dk
Telephone: +45-23-1522651

Received: October 23, 2017
Peer-review started: October 25, 2017
First decision: November 14, 2017
Revised: November 24, 2017
Accepted: December 5, 2017
Article in press: December 5, 2017
Published online: January 14, 2018

Abstract

AIM

To characterize the efficacy of the dual FXR/TGR5 receptor agonist INT-767 upon histological endpoints in a rodent model of diet-induced and biopsy-confirmed non-alcoholic steatohepatitis (NASH).

METHODS

The effects of INT-767 on histological features of NASH were assessed in two studies using *Lep*$^{ob/ob}$ (*ob/ob*) NASH mice fed the AMLN diet (high fat with trans-fat, cholesterol and fructose). In a proof-of-concept

study, *Lep*$^{ob/ob}$ (*ob/ob*) NASH mice were first dosed with INT-767 (3 or 10 mg/kg for 8 wk). A second *ob/ob* NASH study compared INT-767 (3 and 10 mg/kg) to obeticholic acid (OCA) (10 or 30 mg/kg; 16 wk). Primary histological endpoints included qualitative and quantitative assessments of NASH. Other metabolic and plasma endpoints were also assessed. A comparative assessment of INT-767 and OCA effects on drug distribution and hepatic gene expression was performed in C57Bl/6 mice on standard chow. C57Bl/6 mice were orally dosed with INT-767 or OCA (1-30 mg/kg) for 2 wk, and expression levels of candidate genes were assessed by RNA sequencing and tissue drug levels were measured by liquid chromatography tandem-mass spectrometry.

RESULTS

INT-767 dose-dependently (3 and 10 mg/kg, PO, QD, 8 wk) improved qualitative morphometric scores on steatohepatitis severity, inflammatory infiltrates and fibrosis stage. Quantitative morphometric analyses revealed that INT-767 reduced parenchymal collagen area, collagen fiber density, inflammation (assessed by Galectin-3 immunohistochemistry) and hepatocyte lipid droplet area following INT-767 treatment. In a comparative study (16 wk), the FXR agonists OCA (10 and 30 mg/kg) and INT-767 (3 and 10 mg/kg) both improved NASH histopathology, with INT-767 exerting greater therapeutic potency and efficacy than OCA. Mechanistic studies suggest that both drugs accumulate similarly within the liver and ileum, however, the effects of INT-767 may be driven by enhanced hepatic, but not ileal, FXR function.

CONCLUSION

These findings confirm the potential utility of FXR and dual FXR/TGR5 activation as disease intervention strategies in NASH.

Key words: Non-alcoholic steatohepatitis; INT-767; Obeticholic acid; Liver biopsy; FXR; TGR5; Mouse model

Core tip: The studies contained herein evaluated the preclinical efficacy of INT-767, a dual FXR/TGR5 agonist, in a mouse model of diet-induced and biopsy-confirmed non-alcoholic steatohepatitis (NASH). Rigorous analyses for NASH histological endpoints and markers were conducted including blinded qualitative and quantitative scoring using standard microscopy as well as advanced morphometric fibrosis and steatosis features using second harmonic generation imaging and two-photon fluorescence excitation. INT-767 promoted dose-dependent improvements in fibrosis, steatosis, inflammation and ballooning degeneration. The effects of INT-767 and obeticholic acid (OCA) were also compared for histological efficacy, gene expression and tissue distribution. The preclinical data suggest that INT-767 is a more potent FXR receptor agonist, and is expected to have therapeutic effects at lower doses than OCA.

Roth JD, Feigh M, Veidal SS, Fensholdt LKD, Rigbolt KT, Hansen HH, Chen LC, Petitjean M, Friley W, Vrang N, Jelsing J, Young M. INT-767 improves histopathological features in a diet-induced *ob/ob* mouse model of biopsy-confirmed non-alcoholic steatohepatitis. *World J Gastroenterol* 2018; 24(2): 195-210 Available from: URL: http://www.wjgnet.com/1007-9327/full/v24/i2/195.htm DOI: http://dx.doi.org/10.3748/wjg.v24.i2.195

INTRODUCTION

Nonalcoholic fatty liver disease (NAFLD) is considered the hepatic manifestation of the metabolic syndrome, a cluster of closely related clinical features linked to visceral obesity and characterized by insulin resistance, dyslipidemia, and hypertension. While steatosis can be considered a relatively benign liver disease, for reasons that are still incompletely understood, a subgroup of NAFLD patients go on to develop non-alcoholic steatohepatitis (NASH), which is marked by hepatocellular injury, inflammation, and progressive fibrosis. It is estimated that the prevalence of progression from NAFLD to NASH is 10% to 20% in the general population; 37% in the high-risk, severe obese population; and 40% to 55% in patients at tertiary care centers[1]. Several factors have been implicated in the development of NAFLD, including sensitization due to excessive liver triglyceride accumulation coupled with insulin resistance[2].

In addition to their roles in dietary lipid absorption and cholesterol homeostasis, bile acids activate many signaling pathways, including the ligand-activated nuclear farnesoid X receptor FXR[3] and the plasma membrane-bound G protein-coupled receptor TGR5[4,5]. FXR and TGR5 represent attractive targets for the treatment of metabolic and chronic liver diseases. FXR is predominantly expressed in the liver, kidney and intestine, with a major role in controlling bile acid homeostasis. FXR activation suppresses NF-κB–regulated pro-inflammatory genes in hepatocytes and vascular cells, as well as inflammatory mediators such as cyclooxygenase-2 (COX-2) and inducible nitric oxide synthase (iNOS)[6-8]. FXR activation also inhibits production of tumour necrosis factor-alpha (TNF-α) by human peripheral blood mononuclear cells and human monocytes, and inhibits differentiation of human monocytes into dendritic cells[8]. Furthermore, FXR activation inhibits production of TNF-α, interleukin (IL)-17, and interferon gamma (IFN-γ) in lymphocyte-enriched human intestinal lamina propria cells, suggesting that FXR function participates in preserving the intestinal barrier[9]. Although not expressed in hepatocytes, TGR5 is detected in many liver cell types

where it could directly or indirectly modulate hepatic lipid metabolism[10]. TGR5 is highly expressed in Kupffer cells, which are resident liver macrophages[11], and their proinflammatory cytokine secretion has been implicated in the progression of NAFLD[12]. In Kupffer cells, bile acids inhibit lipopolysaccharide-induced cytokine expression *via* TGR5-cAMP-dependent pathways[11]. The increased TGR5 expression in Kupffer cells after bile duct ligation suggests a protective role for TGR5 in obstructive cholestasis, preventing excessive proinflammatory cytokine production and thereby reducing liver injury[11].

INT-767 is a semisynthetic bile acid derivative[13] being developed for the treatment of liver and metabolic diseases and is the first compound described that potently and selectively activates both bile acid receptors (FXR, EC_{50} of approximately 30 nmol/L; TGR5, EC_{50} of 0.6 μmol/L). INT-767 is approximately 300-fold more potent at FXR than the natural homologue, chenodeoxycholic acid (CDCA), and 4- to 12-fold more potent at TGR5 than the natural TGR5 agonist lithocholic acid (LCA)[13]. INT-767 has been profiled in several animal models and shown to improve metabolism and decrease inflammation and fibrosis. For example, INT-767 reduced atherosclerotic plaque formation by preventing hyperlipidemia and inhibiting pro-inflammatory cytokine production in macrophages in a mouse model of hypercholesterolemia[14]. INT-767 also prevented proteinuria, podocyte injury, fibronectin accumulation and TGF-α accumulation associated with age-related kidney disease[15]. Most relevant to NASH was the finding that INT-767 treatment of obese *db/db* mice with NAFLD improved liver histopathology, and modulated intrahepatic macrophage populations to a less inflammatory phenotype[16].

While these results are encouraging, prior studies have not explicitly assessed the effects of INT-767 in mice with biopsy-confirmed histological features of NASH. *Lep*$^{ob/ob}$ (*ob/ob*) mice have been shown to be consistently prone to fibrosis when cholesterol (2%) and trans-fatty acids (45% of total fat amount) are added to a high-caloric diet (termed AMLN diet; Trevaskis, 2012; based on the American Lifestyle-Induced Obesity Syndrome mouse model developed by Tetri and colleagues[17]). With reference to standard clinical practice, biopsy-confirmation procedures have successfully been applied to *ob/ob* mice fed the AMLN diet (hereafter referred to as *ob/ob*-NASH mice) for staging of baseline liver pathology to equalize NASH severity in the experimental groups and perform within-subject comparisons during the course of drug treatment[18,19]. Thus, the present studies evaluated the efficacy of INT-767, administered for 8 wk in *ob/ob*-NASH mice. Rigorous analyses for NASH histological endpoints and markers were conducted including blinded qualitative and quantitative scoring using standard microscopy as well as advanced morphometric fibrosis and steatosis features using second harmonic generation imaging and two-photon fluorescence excitation (SHG/2-PE). The effects of INT-767 and obeticholic acid (OCA) were also compared in a longer-term (16 wk) head-to-head study, as well as in shorter studies (2 wk) comparing hepatic and ileal tissue drug concentration and gene expression profiles.

MATERIALS AND METHODS

Animals

All animal experiments conformed to the internationally accepted principles for the care and use of laboratory animals (license no. 2013-15-2934-00784, The Animal Experiments Inspectorate, Denmark). C57Bl6/J and B6.V-Lep^{ob}/JRj (*ob/ob*) mice (5-6 wk-old) were from Janvier Labs (Le Genest Saint Isle, France) and housed in a controlled environment (12 h light/dark cycle, light on at 3 AM, 21 ℃ ± 2 ℃, humidity 50% ± 10%). Each animal was identified by an implantable microchip (PetID Microchip, E-vet, Haderslev, Denmark). Mice had *ad libitum* access to tap water and either regular rodent chow (C57Bl6/J mice, Altromin 1324, Brogaarden, Hoersholm, Denmark), or a diet high in fat (*ob/ob* mice, 40%, containing 18% trans-fat), 40% carbohydrates (20% fructose) and 2% cholesterol (AMLN diet; D09100301, Research Diets, New Brunswick, NJ)[19]. *ob/ob* mice (n = 87) were fed the AMLN diet for 9 or 15 wk prior to treatment start and during drug treatment. All *ob/ob* animals underwent liver biopsy prior to treatment, see below.

Baseline liver biopsy

The biopsy procedure was applied to all mice approximately three weeks before completion of the dieting period, as detailed previously[19]. In brief, mice were anesthetized with isoflurane, a small abdominal incision in the midline was made, and the left lateral lobe of the liver was exposed. A cone-shaped wedge of liver tissue (50-100 mg) was excised from the distal part of the lobe. The cut surface of the liver was closed by electrosurgical bipolar coagulation. The liver was returned to the abdominal cavity, the abdominal wall was sutured and skin stapled. Carprofen (Rimadyl®, 5 mg/mL, 0.01 mL/10 g; Pfizer, NY) and enrofloxazin (5 mg/mL, 1 mL/kg, *i.p.*) were administered at the time of surgery and at post-operative day one and two. Animals were single-housed after the procedure and recovered for three weeks prior to treatment.

Drug treatment

INT-767 and OCA (Intercept Pharmaceuticals, New York, NY, United States) were dissolved in 0.5% carboxymethyl cellulose, and orally administered in a dosing volume of 5 mL/kg. Animals were stratified (n = 11-12 per group) based on mean fibrosis as assessed by collagen 1a1 staining. In one study, after 15 wk on diet mice were treated with INT-767 (3.0 or 10 mg/kg) for 8 wk. In a second study, after 9 wk on

diet mice were treated with either vehicle, INT-767 (3.0 or 10 mg/kg), or OCA (10 or 30 mg/kg) for 16 wk. A longer duration of administration was selected for this second study to (a) examine the durability of INT-767 NASH histological improvements, and (b) because in our experience OCA requires extended dosing (*e.g.*, at least 12 wk at 10-30 mg/kg) to elicit histological anti-fibrotic responses (data on file) and shorter treatment periods with OCA are not always sufficient to promote antifibrotic effects in *ob/ob*-NASH mice[20]. For analysis of liver and intestinal compound levels, as well as hepatic gene expression, lean C57Bl6 mice received INT-767 (1-3-10-30 mg/kg, PO, QD) or OCA (1-3-10-30 mg/kg, PO, QD) for 14 d.

Body weight and body composition analysis

Body weight was monitored once daily during the intervention period. Whole-body fat mass was analyzed at baseline (week -1) and week 8 of the intervention period by non-invasive EchoMRI scanning using EchoMRI-900 (EchoMRI, Houston, TX).

Plasma and liver biochemistry

Plasma and liver biochemistry was assessed according to methods described in detail previously[19]. Baseline and terminal blood samples from non-fasted mice were assayed for blood glucose levels as well as plasma concentrations of alanine aminotransferase (ALT), aspartate aminotransferase (AST), triglycerides (TG), total cholesterol (TC), and insulin. Terminal liver samples (about 100 mg) were analyzed for TG and TC content.

Oral glucose tolerance test

An oral glucose tolerance test (OGTT) was performed in week 4 of the treatment period according to previously reported procedures[19]. In brief, animals were fasted for 4 h prior to the OGTT. At t = 0 an oral glucose load (2 g glucose/kg) was administered via oral gavage. Succesive blood samples for measuring blood glucose (BG) were collected from the tail vein at t = 0, 15, 30, 60 and 120 min. Glucose area-under-the-curve (AUC) was determined from the sampling period of 0 to 120 min.

Liver histology and digital image analysis

Baseline liver biopsy and terminal samples (both from the left lateral lobe) were fixed overnight in 4% paraformaldehyde. Liver tissue was paraffin-embedded and sectioned (3 μm thickness). Sections were stained with hematoxylin-eosin (HE), PicroSirius Red (PSR, Sigma-Aldrich, Broendby, Denmark), anti-type I collagen (Col1a1; cat. 1310-01, Southern Biotech, Birmingham, AL), anti-galectin-3 (cat. 125402, Biolegend, San Diego, CA, United States), or anti-laminin (cat. Z0097, Agilent Technologies, Glostrup, Denmark) using standard procedures[19]. The NAFLD activity score (NAS) and fibrosis staging system was applied for scoring of steatosis (score 0-3), lobular inflammation (score 0-3), hepatocyte ballooning (score 0-2), and fibrosis (stage 0-4)[21]. Mice with fibrosis stage $\geqslant$ 1 and steatosis score $\geqslant$ 2 were included in the study. Liver sections stained for fat, Col1a1, galectin-3 and laminin were analyzed using digital imaging software (Visiomorph®, Visiopharm, Hørsholm, Denmark). Immunoreactive fractional area was expressed relative (%) to total parenchymal area by subtracting corresponding fat area determined on adjacent HE-sections. In addition, deparaffinized and unstained tissue sections of similar thickness where imaged by second harmonic generation (SHG, label free, specific to collagen 1 and 3, in transmission at 780 nm) and concurrently by 2-photon fluorescence excitation (2-PE at 780 nm, collected at 550 ± 88 nm to delineate the tissue structure). Both optical methods were performed on a mid-throughput, fully automated, nonlinear optical imaging system at 20 X objective and 0.39 μm resolution (Genesis 200®, HistoIndex, Singapore), as described previously[22]. Fat droplets appear as circular dark objects (no intrinsic fluorescence) and can thus be segregated from the parenchyma and quantified (droplet count, area, eccentricity, and size), Collagen fiber data (area, density, reticulation index) were expressed relative (%) to corresponding parenchymal area. The collagen fiber network complexity (reticulation index) was expressed, as the ratio of skeleton fibers nodes to the total length of the equivalent skeleton. Imaging parameters (laser intensity, photomultiplier tube gains, scanning) and image analysis parameters (signal intensity and morphometric thresholding and pruning) where kept constant for the entire study after optimization. SHG was optimized to use the full 8-bit dynamic range of the instrument and avoid saturation. All histological assessments were performed by pathologists and operators blinded to the experimental groups.

LC/MS/MS determination of compound levels in liver and ileum

A mass dependent volume of homogenization solution (seven volumes of 80/20 ACN/HBSS) was added to each tube containing a pre-weighed, intact tissue specimen. Tissue samples were homogenized using an Omni Bead Ruptor 24 tissue homogenizer set to 4 m/s for two cycles of 30 s each. Sample tubes were centrifuged at 3500 rcf for 3 min and a 200 μL aliquot of supernatant was transferred to a 96 deep-well plate. Samples were dried down under nitrogen and reconstituted in 60/40 methanol/10 mmol/L ammonium acetate containing 25 nmol/L of d5-GCA internal standard. Reconstituted samples were transferred to a Millipore 0.45 μm filter plate (Millipore MSHVN45) and filtered into a Costar 3957 plate by centrifugation and sealed with a silicone capmat prior to LC-MS/MS analysis. This extract was injected onto an UHPLC system equipped with a ultra-

Table 1 Effect of 8 wk of treatment with INT-767 on metabolic parameters, non-alcoholic fatty liver disease activity score/fibrosis stage, body weight/composition, and liver weight in *ob/ob*-NASH mice

	Vehicle, (n = 10)	INT-767, 3 mg/kg (n = 10)	INT-767, 10 mg/kg (n = 10)
Baseline plasma ALT (U/L)	577 ± 43.4	552 ± 36.1	498 ± 27.3
Terminal plasma ALT (U/L)	670 ± 58.9	478 ± 33.9	250 ± 21.6[b,f]
Baseline plasma AST (U/L)	436 ± 36.7	421 ± 16.7	359 ± 15.6
Terminal plasma AST (U/L)	552 ± 49.4	447 ± 38.8	257 ± 42.3[e,f]
Baseline plasma TC (mmol/L)	10.3 ± 0.8	10.3 ± 0.8	11.1 ± 0.3
Terminal plasma TC (mmol/L)	10.7 ± 0.5	9.2 ± 0.3	7.2 ± 0.4[e,f]
Baseline plasma TG (mmol/L)	0.8 ± 0.0	0.8 ± 0.1	0.8 ± 0.1
Terminal plasma TG (mmol/L)	0.7 ± 0.0	0.6 ± 0.0	0.6 ± 0.1
Terminal liver TC (mg/g tissue)	32.9 ± 1.7	24.0 ± 1.1[d]	18.0 ± 1.5[f]
Terminal liver TG (mg/g tissue)	233 ± 12.3	229 ± 15.4	149 ± 14.0[d]
Fasting blood glucose (week 4, mmol/L)	7.6 ± 0.1	8.2 ± 0.2	8.0 ± 0.3
OGTT, glucose AUC (week 4, mmol/L × min)	1318 ± 61	1304 ± 38	1417 ± 78
Fed blood glucose (week 8, mmol/L)	7.1 ± 0.2	6.8 ± 0.2	7.3 ± 0.3
Fed plasma insulin (week 8, pmol/L)	567 ± 133	482 ± 122	799 ± 229
Baseline steatosis score	3.0 ± 0.0	2.9 ± 0.1	2.9 ± 0.1
Terminal steatosis score	3.0 ± 0.0	3.0 ± 0.0	1.8 ± 0.2[f]
Baseline inflammation score	2.5 ± 0.1	3.0 ± 0.0	3.0 ± 0.0
Terminal inflammation score	2.3 ± 0.1	2.2 ± 0.2	1.0 ± 0.1[f]
Baseline ballooning degeneration score	0.6 ± 0.1	0.7 ± 0.1	0.8 ± 0.1
Terminal ballooning degeneration score	0.9 ± 0.1	0.7 ± 0.1	0.2 ± 0.1[f]
Baseline NAFLD activity score (NAS)	6.1 ± 0.2	6.3 ± 0.2	6.4 ± 0.2
Terminal NAFLD activity score (NAS)	6.2 ± 0.2	5.9 ± 0.2	3.0 ± 0.3[f]
Baseline fibrosis stage	2.7 ± 0.2	2.6 ± 0.1	2.6 ± 0.1
Terminal fibrosis stage	2.7 ± 0.1	2.5 ± 0.1	1.6 ± 0.1[f]
Terminal steatosis (% area)	41.1 ± 1.0	40.6 ± 1.6	24.8 ± 2.3[f]
Terminal fibrosis (% area)	15.9 ± 0.9	13.6 ± 0.8	8.9 ± 0.6[f]
Baseline BW (g)	49.8 ± 0.7	48.2 ± 1.0	49.4 ± 1.3
Terminal BW (g)	54.6 ± 0.8	52.6 ± 0.8	51.3 ± 1.8
Body weight change (%, relative to day 0)	109 ± 1.3	107 ± 2.1	103 ± 2.3
Baseline whole-body lean mass (g)	14.0 ± 0.4	14.6 ± 0.3	14.4 ± 0.4
Terminal whole-body lean mass (g)	17.3 ± 0.4	17.6 ± 0.5	17.2 ± 0.2
Baseline whole-body lean mass (% of BW)	28.2 ± 0.6	30.3 ± 0.6	29.1 ± 0.6
Terminal whole-body lean mass (% of BW)	31.9 ± 0.6	33.9 ± 0.9	33.6 ± 0.8
Baseline whole-body fat mass (g)	18.5 ± 0.4	18.5 ± 0.7	19.5 ± 0.7
Terminal whole-body fat mass (g)	22.5 ± 0.4	21.0 ± 0.7	19.3 ± 0.7[e]
Baseline whole-body fat mass (% of BW)	37.2 ± 0.7	38.4 ± 1.2	39.4 ± 0.6
Terminal whole-body fat mass (% of BW)	41.4 ± 0.5	40.4 ± 0.9	37.5 ± 0.7[e]
Terminal liver weight (g)	5.4 ± 0.2	4.9 ± 0.1	4.1 ± 0.1[f]
Terminal liver weight (% of BW)	9.8 ± 0.3	9.4 ± 0.2	8.0 ± 0.3[d]

Morphometric scores were analyzed by a χ^2 test compared to vehicle. All other data were analyzed by a two-way ANOVA with Bonferroni's *post-hoc* test ([a]P < 0.05, [b]P < 0.01, [e]P < 0.001; *vs* baseline. [c]P < 0.05, [d]P < 0.01, [f]P < 0.001, *vs* vehicle).

high resolution, accurate mass, mass spectrometer (UHRAM) (Thermo Fisher Scientific *Q* Exactive with Ion Max M2 with HESI-Ⅱ probe) detector operated in negative electrospray mode. Separation of test article from extracted matrix materials was accomplished using a Thermo Fisher Hypersil Gold C18 column (1 mm x 100 mm, 1.9 μm particle size) operating at 45 ℃. The gradient mobile phase system consisted of 0.25 mmol/L ammonium acetate in 40% methanol (mobile phase A) and 0.25 mmol/L ammonium acetate in 95% methanol (mobile phase B) at a total flow rate of 0.100 mL/min.

Twenty analytical runs were performed during the study sample analysis. Calibration standards, prepared in matrix matched mouse control tissues purchased from BioreclamationIVT (Baltimore, MD), were used to construct standard curves for all analytes. Typically, quadratic weighted (1/x) regression analysis of peak area ratio *vs* theoretical concentration was used to produce calibration curves.

RNA sequencing

Hepatic and ileal transcriptome analysis was performed by RNA sequencing on RNA extracts from terminal liver samples, as described[19]. RNA sequence libraries were prepared with NeoPrep (Illumina, San Diego, CA, United States) using Illumina TruSeq stranded mRNA Library kit for NeoPrep (Illumina, San Diego, CA, United States) and sequenced on the NextSeq 500 (Illumina, San Diego, CA, United States) with NSQ 500 hi-Output KT v2 (75 CYS, Illumina, San Diego, CA, United States). Reads were aligned to the GRCm38 v84 Ensembl Mus musculus genome using STAR v.2.5.2a with default parameters[23]. Differential gene

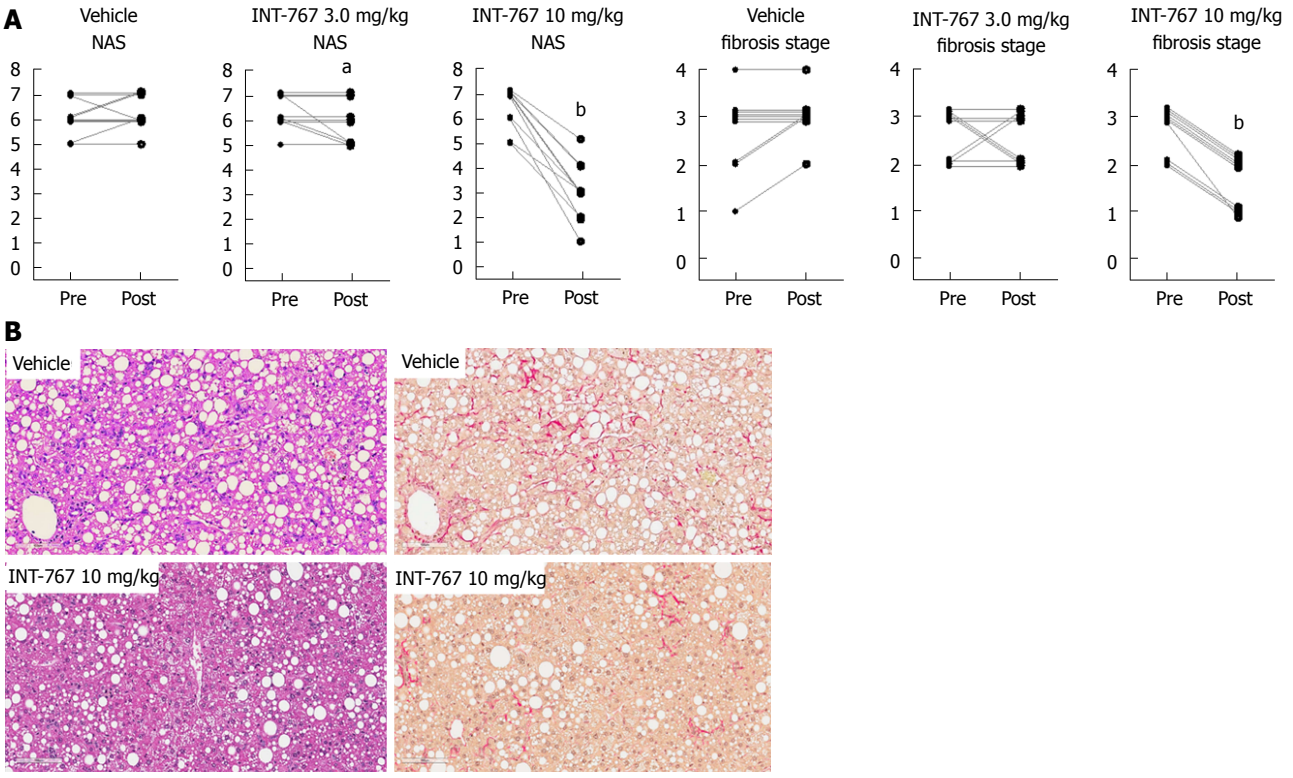

Figure 1 INT-767 treatment for 8 wk improves liver histopathology in *ob/ob*-NASH mice with biopsy-confirmed liver pathology. A: Composite NAS and fibrosis stage before and after treatment intervention; B: Representative HE and PSR stainings. $^{a}P < 0.05$, $^{b}P < 0.001$ (χ^2 test, *vs* vehicle controls).

expression analysis was performed with DEseq215[24].

Statistical analysis

All data were analyzed using GraphPad Prism 5.0 (GraphPad Software, La Jolla, CA, United States). Results are presented as mean ± SE. A chi-square (χ^2) test was used to test for within-subject changes in qualitative histology scores before and after treatment, compared to vehicle controls. Responders were defined as having a $\geqslant$ 1 point change in the indicated score. An unpaired two-tailed *t-test* was applied to quantitative histological analyses after treatment. A two-way ANOVA with Bonferroni's post-hoc test was used for analysis of changes in gene expression and quantitative histology analytes (fractional area of fat, galectin-3, and Col1a1) before and after treatment, compared to vehicle controls. A *P*-value less than 0.05 was considered statistically significant.

RESULTS

INT-767 improves liver histopathology after 8 wk of treatment in ob/ob-NASH mice

All *ob/ob*-NASH mice included in the experiment had liver biopsy-confirmed NASH (NAS 5-7) and fibrosis (stage 1-4) prior to initiation of treatment (Table 1).

INT-767 promoted dose-dependent improvements in liver histopathology after eight wk of treatment in *ob/ob*-NASH mice. INT-767 10 mg/kg significantly reduced steatosis, inflammation and hepatocyte ballooning degeneration scores compared to vehicle controls (Table 1). All INT-767 (10 mg/kg) treated mice exhibited reductions in NAS and fibrosis stage (Figure 1, Table 1). In contrast, *ob/ob*-NASH control mice maintained composite NAS and fibrosis scores compared to pre-treatment levels. INT-767 also reduced quantitative hepatic collagen and fat, as indicated by lowered Col1a1 immunoreactivity (Figure 2B) and liver fat area (Figure 3B). This reduction of collagen and fat by INT-767 was also shown in the IHC staining images (Figures 2A and 3A, respectively) and confirmed by label free SHG/2-PE images and processed images for fat content (Figures 2C and 3C, respectively).

SHG/2-PE morphometric assessments of collagen were positively correlated with Col1a1 assessment by immunohistochemistry (r^2 = 0.88, P <0.0001) and demonstrated that INT-767 predominantly impacted collagen fiber density, but not collagen fiber network complexity (reticulation index, Figure 2D). With respect to steatosis, INT-767 reduced mean fat droplet area, but not droplet count (Figure 3D). The size distribution of fat droplets in INT-767 treated *ob/ob*-NASH mice were left-shifted, suggesting a vesicular fat redistribution towards a less macro-steatotic phenotype (Figure 4).

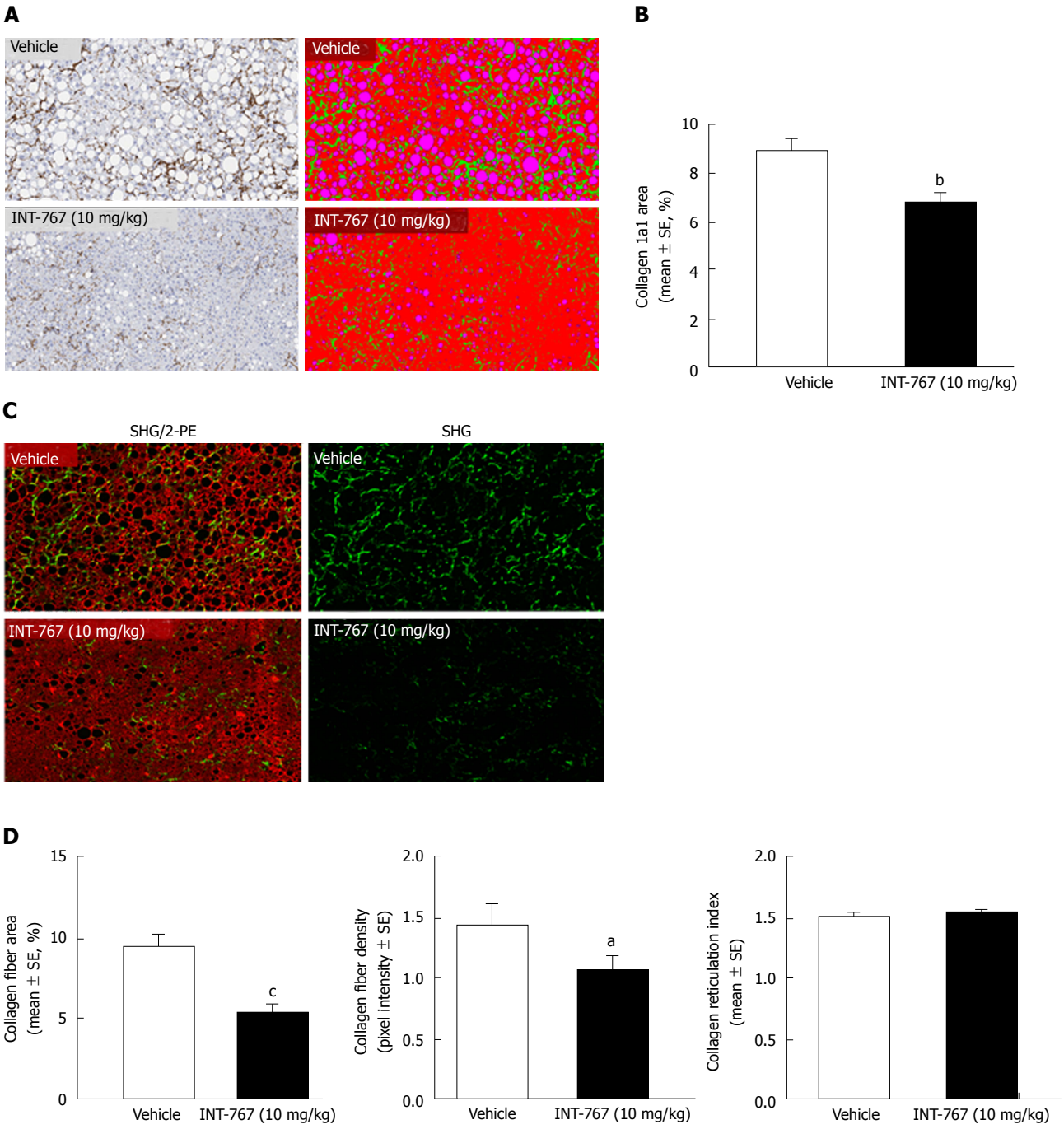

Figure 2 INT-767 treatment for 8 wk reduces hepatic collagen deposition in *ob/ob*-NASH mice with biopsy-confirmed liver pathology. A: Collagen 1a1 (immunohistochemistry); B: Fractional area of collagen (immunohistochemistry); C: Label free SHG/2-PE images for collagen fiber deposition (green) in hepatic parenchyma (red). Data are expressed as % of total parenchymal area (subtraction of fat area); D: Fractional area of collagen fiber, collagen fiber density, and collagen fiber reticulation index (SHG analysis). $^{a}P < 0.05$, $^{b}P < 0.01$, $^{c}P < 0.001$ (unpaired *t*-test).

In line with these morphometric changes, and similar to PPAR agonists[25], INT-767 10 mg/kg significantly reduced mRNA levels of cell death-inducing DNA fragmentation factor alpha-like effector c (CIDEC; a lipid-droplet associated protein that promotes intracellular storage) relative to vehicle (in RPKM, 109.4 ± 10 (vehicle) *vs* 40.8 ± 10.8 (INT-767), $P = 0.0018$).

The liver histological changes with INT-767 (10 mg/kg) treatment were accompanied by significant improvements in liver enzymes (ALT and AST). INT-767 also reduced whole-body fat mass (without changing body weight), hepatomegaly and intrahepatic concentrations of TC and TG (Table 1). In addition, INT-767 reduced terminal liver concentrations of TC and TG, and plasma TC (Table 1).

INT-767 and obeticholic acid show similar hepatic and ileal distribution in C57Bl6 mice

Hepatic and ileal concentrations of INT-767 and OCA

Table 2 INT-767 and obeticholic acid improve liver histomorphology in *ob/ob*-NASH steatohepatitis mice with biopsy-confirmed liver pathology

Treatment	Fibrosis stage			NAS		
	No improvement	With improvement	% improving[1]	No improvement	With improvement	% improving[1]
Vehicle (n = 11)	11	0	0%	11	0	0%
OCA 10 mg/kg (n = 12)	10	2	17%	8	4	33%
OCA 30 mg/kg (n = 11)	7	4	36%[a]	0	11	100%[a]
INT-767 3.0 mg/kg (n = 12)	12	0	0%	7	5	42%[a]
INT-767 10 mg/kg (n = 11)	2	9	82%[a]	0	11	100%[a]

Subjects (%) achieving > [1]points improvement in score from baseline; [a]$P < 0.05$ *vs* vehicle (χ^2 test).

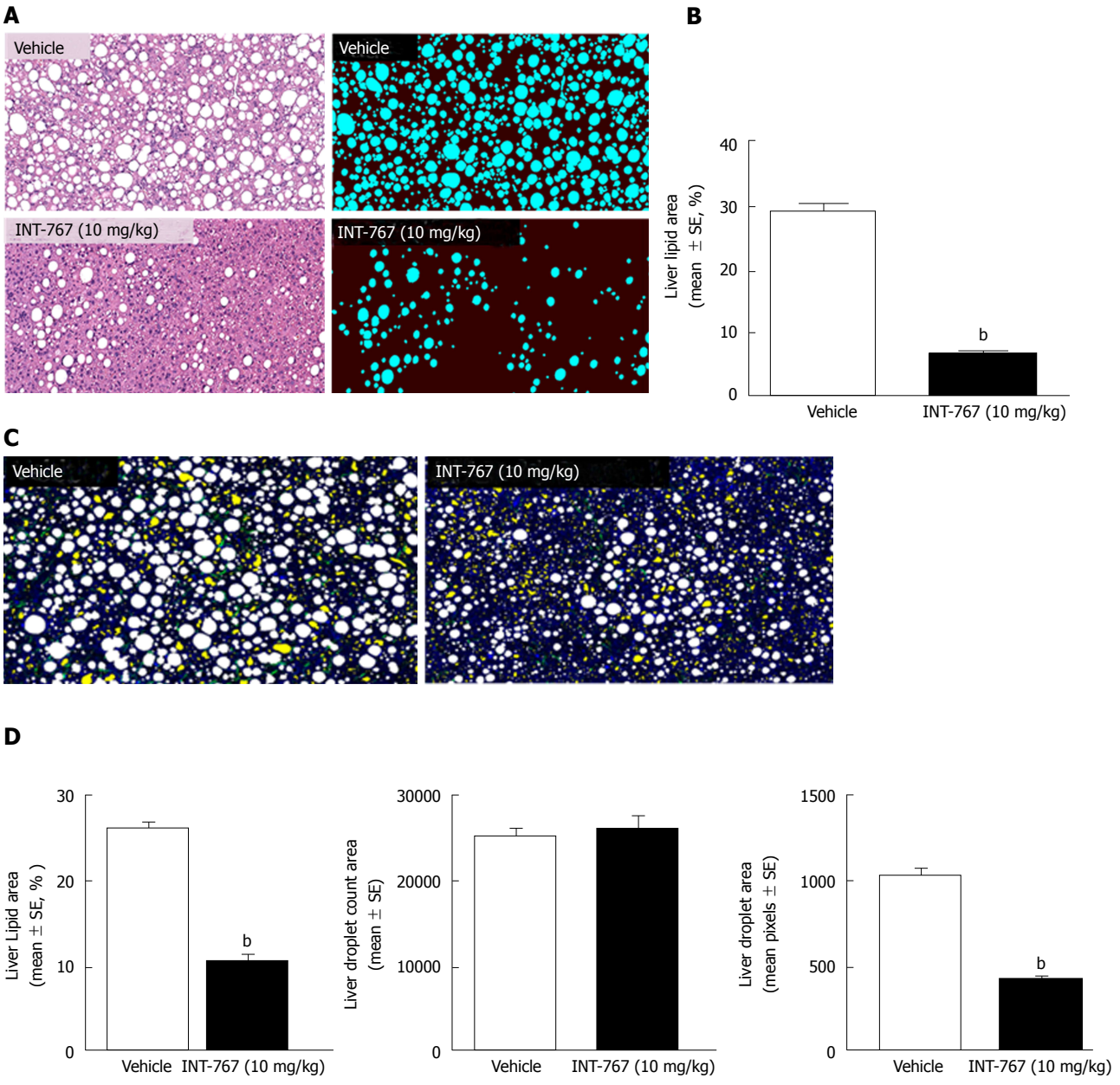

Figure 3 INT-767 treatment for 8 wk reduces hepatic lipid deposition in *ob/ob*-NASH mice with biopsy-confirmed liver pathology. A: Liver lipid (HE staining); B: Fractional area of liver fat (HE staining); C: Processed (color coded) images to display hepatic lipid content. Lipid droplets (white), rejected structures (yellow), collagen (green), auto-fluorescence (blue); D: Fractional area of liver lipid area ratio (%), lipid droplet number (count in 15 mm^2 tissue area), and lipid droplet area (1 pixel = 0.39 μm, 2-PE analysis). [b]$P < 0.001$ (unpaired t-test).

Table 3 INT-767 and obeticholic acid improve quantitative liver histopathology in *ob/ob*-NASH mice

Treatment	Lipid (steatosis)		Galectin-3 (inflammation)		Collagen 1a1 (fibrosis)	
	% fractional area					
	Before treatment	After treatment	Before treatment	After treatment	Before treatment	After treatment
Vehicle (n = 11)	33.0 ± 0.9	30.4 ± 0.9	5.7 ± 0.5	7.8 ± 0.5	1.2 ± 0.3	12.1 ± 0.4
OCA 10 mg/kg (n = 12)	33.4 ± 0.8	31.8 ± 0.4	5.5 ± 0.3	5.0 ± 0.2[a]	0.9 ± 0.1	9.0 ± 0.6[a]
OCA 30 mg/kg (n = 11)	32.2 ± 1.1	22.7 ± 1.0[a]	5.5 ± 0.4	4.0 ± 0.4[a]	1.2 ± 0.2	8.0 ± 0.7[a]
INT-767 3.0 mg/kg (n = 12)	33.0 ± 0.9	29.4 ± 1.3[a]	5.6 ± 0.5	5.4 ± 0.2[a]	1.2 ± 0.2	8.5 ± 0.6[a]
INT-767 10 mg/kg (n = 11)	33.7 ± 0.8	12.5 ± 1.5[a]	5.6 ± 0.3	2.9 ± 0.1[a]	0.9 ± 0.2	5.0 ± 0.3[a]

Fractional area (mean ± SE) at the end of study; [a]P < 0.05 *vs* vehicle (two-way ANOVA, Bonferroni's *post-hoc* test).

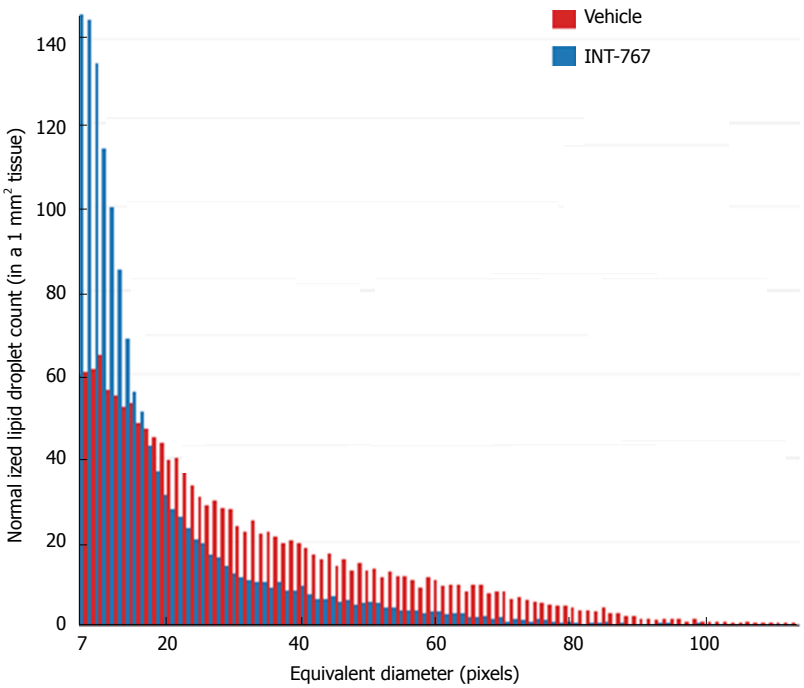

Figure 4 Histogram depicting lipid droplet size distribution in INT-767 *vs* vehicle treated *ob/ob*-NASH mice. The "equivalent diameter" is the diameter of a circle of equivalent area as the one measured on the image (often not a perfect circle). Unit is in pixels, with 1 pixel = 0.39 μm.

were determined after 14 d of dosing (1-30 mg/kg, PO) in chow-fed C57Bl6 mice only. Both compounds showed similar dose-dependent increases in hepatic and ileal exposure. For both compounds, ileal drug concentrations were approximately two-fold higher compared to the liver (Figure 5).

Impact on INT-767 and obeticholic acid on ileal and hepatic FXR target gene expression in C57Bl6 mice

Based on RNAseq data, prototypic FXR target genes were selected for analysis upon acute dosing of INT-767 and OCA (1-30 mg/kg, PO) in C57Bl6 mice. Both INT-767 and OCA regulated hepatic FXR genes, however, INT-767 more strongly regulated these genes at the highest dose administered (Figure 6A-D). By contrast, within the ileum, OCA had more pronounced effects that INT-767 to stimulate SHP and FGF-15 (Figure 6E and F).

INT-767 shows greater efficacy than obeticholic acid on liver histopathology after 16 wk of treatment in ob/ob-NASH mice

Given that INT-767 showed similar efficacy on hepatic FXR target gene expression, albeit at a lower dose compared to OCA (see above), a comparative study on the pharmacodynamics of potency-adjusted doses of INT-767 (3.0, 10 mg/kg) and OCA (10, 30 mg/kg) was performed in *ob/ob*-NASH mice. To better capture effects on progression of fibrosis, treatment was initiated in *ob/ob*-NASH mice fed AMLN diet for 6 wk (*vs* 12 wk in the previous study) and these mice presented with milder baseline NASH (NAS ⩾ 4, fibrosis ⩾ stage 1). All tested doses of INT-767 and OCA significantly reduced composite NAS, as compared to baseline (Figure 7 and 8). Administration of the highest doses of each compound effectively reduced NAS in all treated *ob/ob*-NASH mice (Table 2), but also significantly

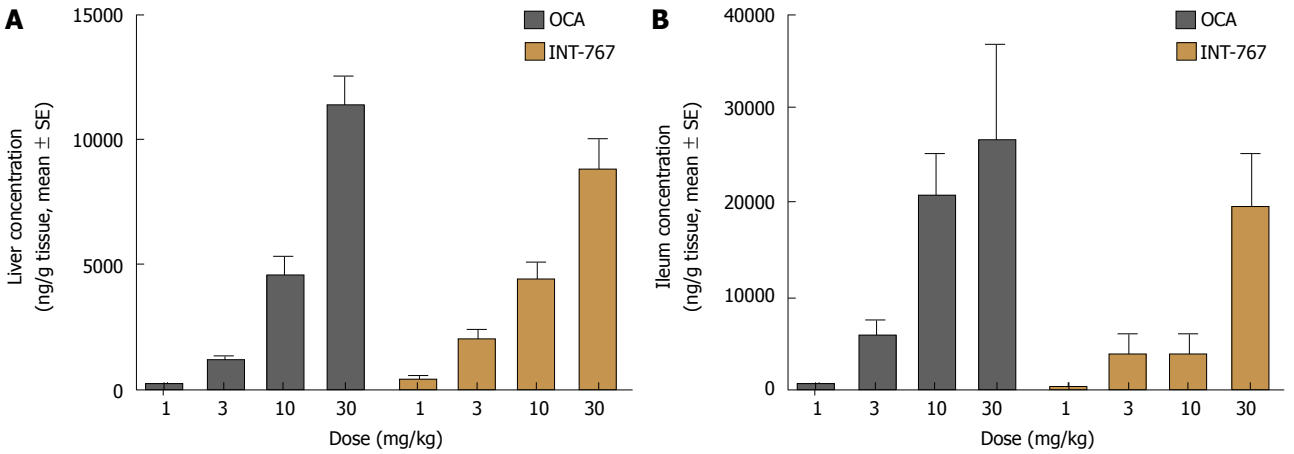

Figure 5 INT-767 and obeticholic acid (OCA) distribute similarly in the liver and ileum after 2 wk of administration in lean C57Bl/6 mice. A: Liver concentration; B: Ileum concentration.

reduced fibrosis scores in the animals (Figure 7 and 8). The ratio of mice achieving > 1 points improvement in score from baseline were 82% (9/11 animals, INT-767 10 mg/kg) and 57% (4/7 animals, OCA 30 mg/kg), see Table 2.

INT-767 and OCA showed corresponding effects on quantitative measures (fractional area) of hepatic steatosis (lipid %), inflammation (galectin-3 %), and collagen deposition (Col1a1 %) in *ob/ob*-NASH mice. INT-767 showed consistently greater maximal effects on all three parameters, as compared to OCA (Figure 9, Table 3).

DISCUSSION

Multiple methods were used to rigorously characterize the effects of INT-767 on liver histopathology in a preclinical mouse model of NASH, alone and in comparison, with OCA, and to determine potential mechanisms underlying INT-767 efficacy on NASH pathology.

The NAS system and fibrosis staging (developed by the NASH Clinical Research Network[21]) is a validated morphometric system for monitoring histopathological changes in clinical trials for NASH. In the clinic, the incorporation of a baseline biopsy affords the opportunity to further characterize within-subject changes in these parameters, and therefore also applied to *ob/ob*-NASH mice in the present study. Hepatopathology was evident in *ob/ob*-NASH mice maintained on AMLN diet for 12 wk. Consistent with previous publications using this model[18,19,26], *ob/ob*-NASH mice present with marked steatosis and inflammation, mild-stage ballooning and moderate-marked grades of fibrosis.

In the initial 8-wk dose-response study, INT-767 10 mg/kg reduced fibrosis stage (approximately 1 point) and total NAS (approximately 3 points). There was a high responder rate for improvement of steatosis (8/10 mice), inflammation (10/10 mice), hepatocyte ballooning (6/10 mice) scores, and fibrosis stage (10/10 mice). Eight weeks of treatment with INT-767 3 mg/kg was a subthreshold dose for eliciting changes in liver histology in *ob/ob*-NASH mice, which is consistent with low levels of hepatic and ileal exposure of INT-767 (see below) and minimal transcriptional regulation of FXR target genes. Although 3 mg/kg INT-767 was ineffective when initiated after 12 wk on the diet, some efficacy was noted when this lower dose was initiated after 6 wk on the diet and over a longer duration in *ob/ob*-NASH mice (OCA *vs* INT-767 comparison study). In sum, blinded qualitative histological assessments of NAS and fibrosis confirmed the efficacy of INT-767 in diet-induced and biopsy-confirmed NASH mice.

Although not validated for preclinical use, the human NAS system is largely reproducible in NAFLD mouse models and has been applied in the preclinical assessment of liver histological responses to test compounds[27]. Despite widespread use, inherent limitations of this method are associated with the subjective qualitative scoring technique (*e.g.*, intra- and inter-observer error, mistaking stage scores for measurements), misapplication of statistical analyses (*e.g.*, ANOVAs on non-numerical data), and categorical data tend to provide a relative narrow window for detecting treatment effects[28]. Additionally, qualitative scoring of disease stage largely assesses architectural changes but is not a quantitative measurement of the degree of fibrosis. Given the link between fibrosis progression and long-term outcomes in NASH[29], more detailed and quantitative assessments of fibrosis are warranted.

To gain further insight into INT-767-induced histological improvements in *ob/ob*-NASH mice, morphometric features of fibrosis were measured using SHG/2-PE microscopy[22]. SHG-2PE is a label-free sensitive imaging method for the detection of tissue structural dissymmetry and for imaging and quantitative assessment of collagen fiber specifically with non-centrosymmetric structures like collagen 1 and 3 which

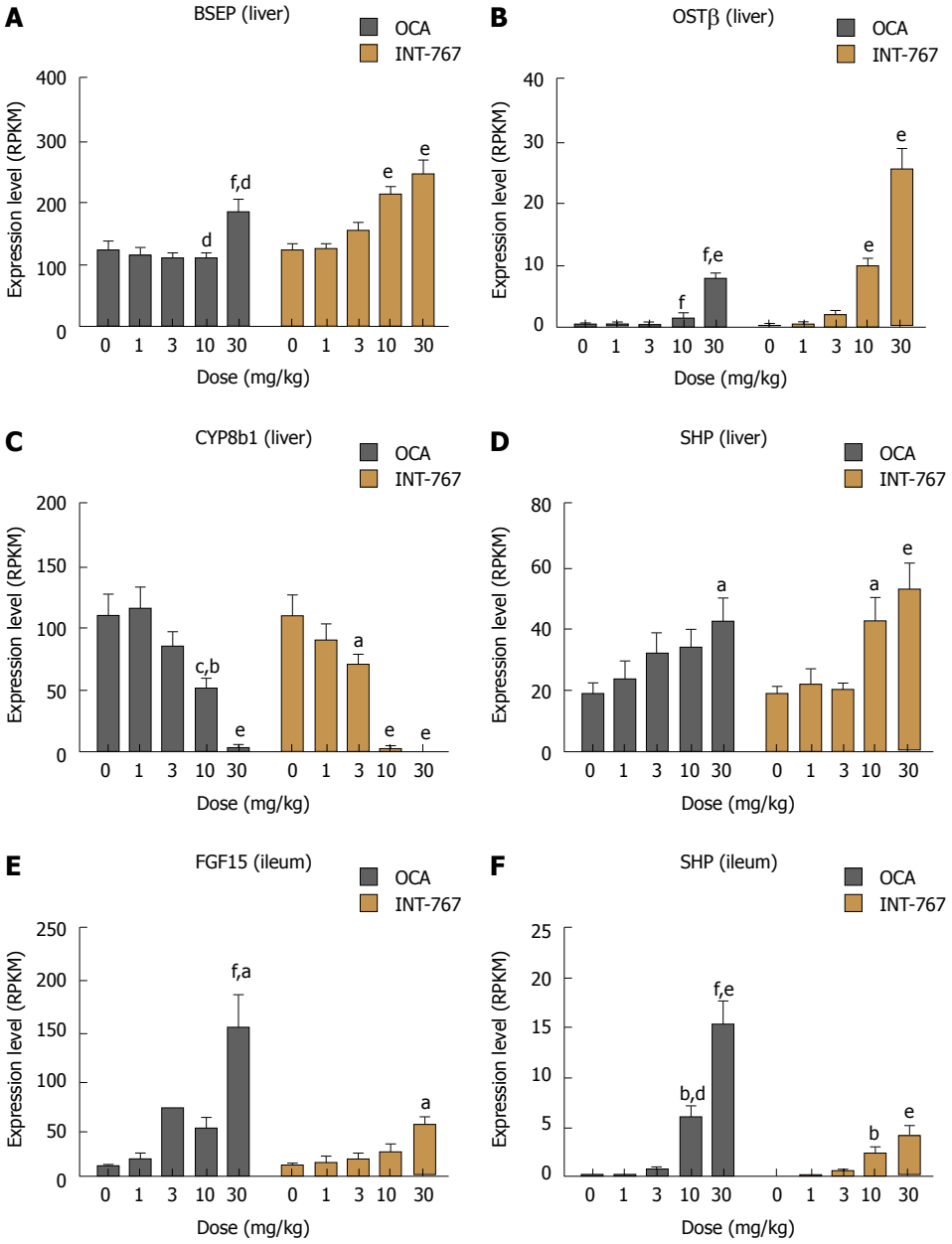

Figure 6 Obeticholic acid (OCA) and INT-767 modulate ileal and hepatic FXR target gene expression to a similar degree after 2 wk of dosing in lean C57Bl/6 mice. A-D: Hepatic expression of BSEP, OST, CYP8b1, and SHP; E and F: Ileal mRNA expression of FGF-15 and SHP. [a]$P < 0.05$, [b]$P < 0.01$, [e]$P < 0.001$ *vs* no treatment (dose = 0); [c]$P < 0.05$, [d]$P < 0.01$, [f]$P < 0.001$ *vs* corresponding INT-767 dose (two-way ANOVA with Bonferroni's *post-hoc* test).

are key contributors for hepatic fibrosis[30]. Accordingly, a significant correlation was observed between quantitative liver collagen levels (expressed as percent collagen area of total parenchymal area) using label free SHG and the collagen 1a1 immunoreactivity. SHG imaging also demonstrated that INT-767 reduced the intensity of the collagen fiber signal (collagen fiber density), but did not affect collagen network complexity (reticulation index).

The present studies also included biochemical assessments, HE staining and label-free SHG/2-PE analyses to determine effects of INT-767 on hepatic lipid parameters. INT-767 dose-dependently reduced hepatic total cholesterol and liver triglyceride levels. In addition to improving steatosis scores, liver lipid fractional area (HE staining) was also markedly reduced by INT-767. Quantitative morphometric analyses by SHG/2-PE imaging confirmed this observation, and revealed that INT-767 significantly reduced vesicular lipid droplet size with a clear shift towards smaller size lipid droplet across the range of possible droplet diameters. These findings are consistent with FXR/TGR5 stimulation of hepatic fatty acid β-oxidation and reduced triglyceride synthesis, and mirror anti-steatotic effects of INT-767 reported within other models of NAFLD[13,16] and are reminiscent of some of the lipid-lowering effects of PPARs. As macrovesicular steatosis positively correlated to the severity of lobular inflammation in NASH patients[31], as well as impaired hepatic microcirculation in experimental NASH[32], the lowering of lipid droplet

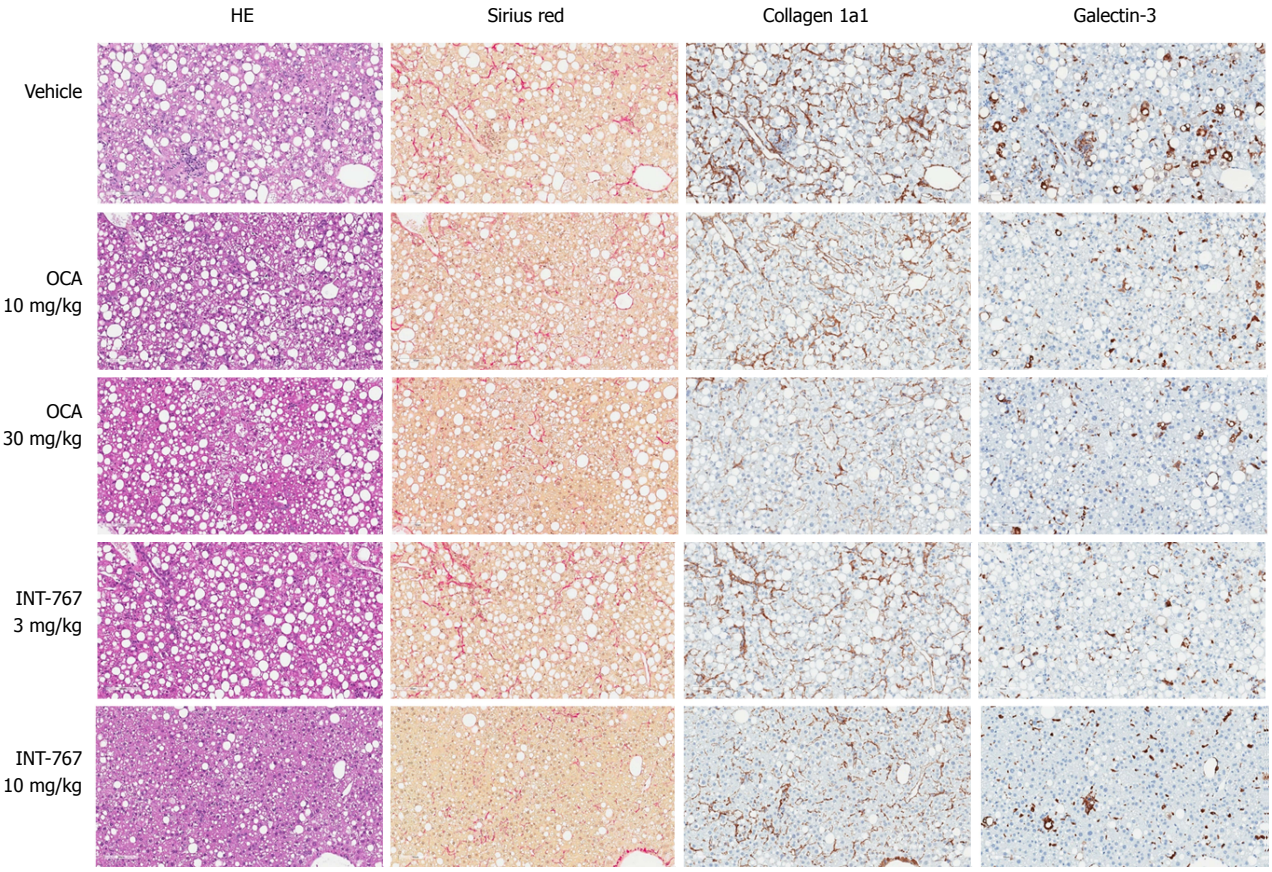

Figure 7 INT-767 and obeticholic acid (OCA) treatment for 16 wk improves liver histopathology in *ob/ob*-NASH mice with biopsy-confirmed liver pathology. Representative hematoxylin-eosin (HE), picro-Sirius red, collagen 1a1 and galectin-3 stainings; NASH: Non-alcoholic steatohepatitis.

area (diameters) by INT-767 is suggestive of improved liver function in *ob/ob*-NASH mice.

The mechanism of action and relative efficacy of INT-767 and OCA was explored. When drawing mechanistic conclusions an important first step is to account for the distribution of each drug within target tissues. INT-767 and OCA are semisynthetic bile acids and exhibits a similar pharmacokinetic profile as endogenous bile acids. These compounds are absorbed from the small intestine, transported into the liver where they undergo biliary excretion and enterohepatic recirculation and are ultimately excreted in the feces. Both compounds were administered to lean mice once daily for two weeks (a duration sufficient to achieve steady-state) and drug levels within the liver and ileum were measured. Both drugs achieved similar levels within similar dose ranges. Likewise, except for the 10 mg/kg dose, levels of INT-767 and OCA were similar within the ileum. Thus, interpretation of differences in hepatic and ileal gene expression within these samples are unlikely to be explained by differences in INT-767 *vs* OCA distribution.

In vivo gene expression studies revealed that relative to OCA, INT-767 regulated hepatic FXR target genes to a greater degree at equivalent doses. These include upregulation of the bile salt efflux transporter *BSEP*, critically involved in the secretion of bile salts into bile, and the organic solute transporter *OSTβ*, which mediates both cellular efflux and uptake of bile acids. Additionally, the cytochrome P450 Family 8 Subfamily B Member 1 (*Cyp8b1*, whose catalytic activity determines solubility of cholesterol in bile by controlling the ratio of cholic acid over CDCA synthesis) was more potently downregulated by INT-767 relative to OCA. These findings are not surprising, given that *in vitro*, INT-767 (EC_{50} approximately 30 nmol/L) is about 300-fold more potent than CDCA and 3-fold more potent than OCA at the FXR receptor[13].

Likewise, for TGR5, INT-767 (EC_{50} approximately 0.63 μmol/L) is about 12-fold more potent than the endogenous TGR5 agonist LCA (EC_{50} approximately 8 μmol/L) and comparable to the selective TGR5 agonist INT-777 (EC_{50} 0.9 μmol/L[13]). Unfortunately, we were unable to demonstrate specific functional or differential activation of TGR5 with INT-767 and OCA; TGR5 hepatic and ileal mRNA target genes are non-specific and future studies should consider examining effects in other TGR5 expressing tissues, such as brown adipose, pancreas or colon, using techniques more appropriate for assessing GPCR activation[5].

Intestinal FXR activation also impacts hepatic signaling events, and liver transcriptome analysis in chow-fed C57Bl6/J mice revealed an important difference between INT-767 and OCA. Fibroblast growth

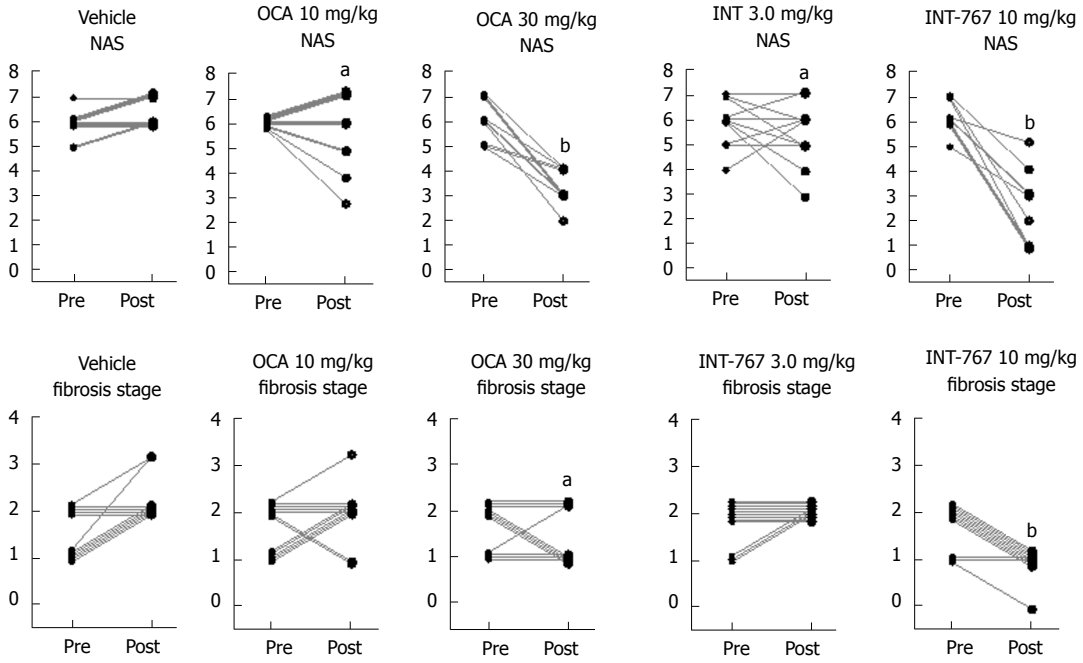

Figure 8 INT-767 and obeticholic acid (OCA) treatment for 16 wk improves liver histopathology in *ob/ob*-NASH mice with biopsy-confirmed liver pathology. Composite NAS and fibrosis stage before and after treatment intervention. [a]$P < 0.05$, [b]$P < 0.001$ (χ^2 test, *vs* vehicle controls), NASH: Non-alcoholic steatohepatitis.

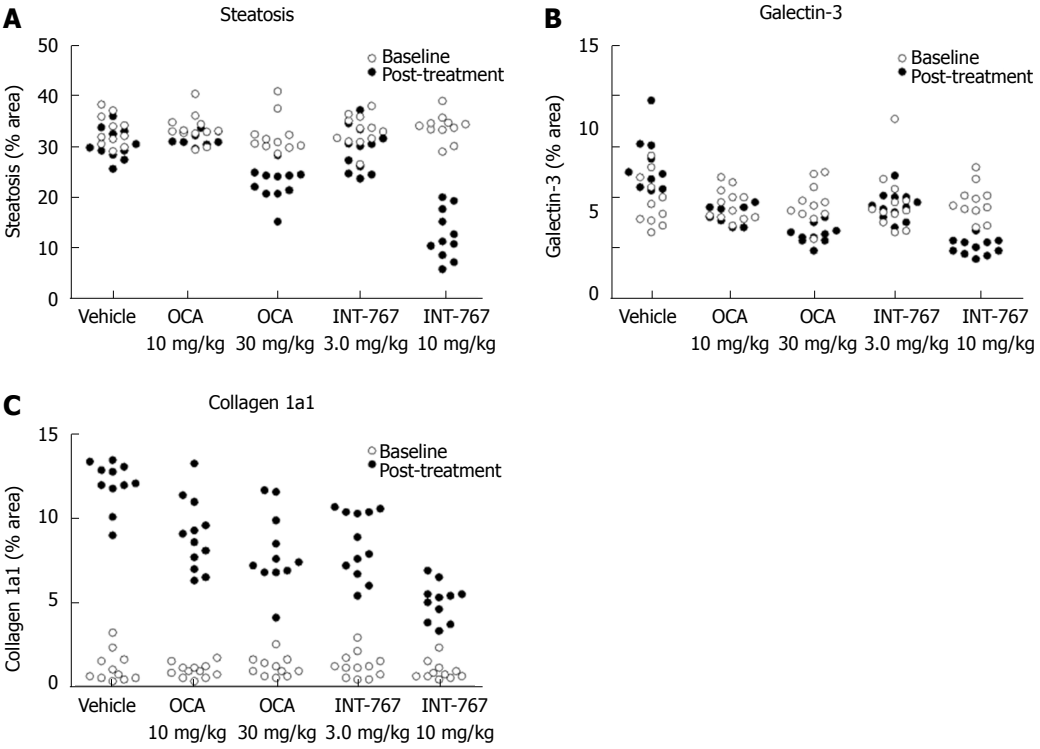

Figure 9 INT-767 or obeticholic acid treatment for 16 wks improves hepatic fat deposition, collagen 1a1 and galectin-3 levels in *ob/ob*-NASH mice with biopsy-confirmed liver pathology. Data are indicated before (baseline) and after treatment intervention. A: Fractional area of fat (HE staining); B: Galectin-3; C: Collagen 1a1. Data are expressed as % of total parenchymal area (subtraction of fat area); NASH: Non-alcoholic steatohepatitis.

factor 15 (FGF-15, equivalent to human FGF-19) is highly expressed the small intestine and upon secretion, circulates to the liver and attenuates bile acid production *via* binding to the β-Klotho receptors located on the surface of hepatocytes and other endothelial cells[33]. It is therefore argued that enhanced gut-liver FGF-15/19 signaling could contribute to anti-NASH effects of bile acid sensing receptors[34,35]. However, the same mice that experienced robust hepatic activation, INT-767 only modestly increased ileal FGF-15 mRNA compared to OCA. These findings suggest that relative to OCA, hepatic FXR signaling may be a greater driver

of INT-767 induced anti-NASH effects. At present, we do not have a mechanistic explanation as to why INT-767 exerts divergent effects on ileal FXR target genes despite being more potent than OCA and demonstrating clear accumulation within the target tissue.

An extended dosing period (16 wk) was employed in *ob/ob*-NASH mice to assess the durability of INT-767-induced anti-NASH efficacy as well as comparing the efficacy of INT-767 and OCA at equipotent doses for FXR activation. After 16 wk of treatment OCA and INT-767 significantly improved all histological parameters relative to vehicle control. In general, the drug treatment effects were dose dependent and the high dose of INT-767 outperformed the high dose of OCA. These findings confirm durable histological benefits of INT-767 with continued drug administration in a preclinical model of NASH and suggest that INT-767 may exert greater efficacy than OCA at both matched and (*in vitro*) potency-adjusted doses.

The therapeutic armamentarium for NAFLD and NASH is limited largely to lifestyle modifications and treatment of concurrent conditions, such as diabetes and obesity, with no currently approved medical treatments for the disease. Based on the nonclinical data presented herein, INT-767 is a more potent FXR receptor agonist, and is expected to have a therapeutic effect at lower doses than OCA. Ongoing clinical studies will allow a more comprehensive assessment of the benefit-risk profile of INT-767 for the treatment of NASH.

ARTICLE HIGHLIGHTS

Research background

Studies within this manuscript detail the efficacy of the dual *in vitro* FXR/TGR5 agonist INT-767 upon multiple histological endpoints in a mouse model of diet-induced non-alcoholic steatohepatitis (NASH). Prior pharmacology studies using INT-767 had not been conducted in models of established and biopsy-confirmed NASH with sufficient fibrosis.

Research motivation

INT-767 is in early clinical development for NASH. These preclinical studies provide proof-of-concept for efficacy in NASH and preclinical superiority relative to obeticholic acid (OCA; an FXR agonist in late stage development for NASH). The present studies also aimed to shed light on the impact of INT-767 on morphometric features of steatosis (droplet size and number) and fibrosis (fiber density) using quantitative histological methods.

Research objectives

The primary objective was to characterize improvements in NASH histopathology using qualitative (*e.g.*, NAS stage scoring for steatosis, inflammation, and ballooning and fibrosis) and quantitative (percent fractional area; %FA) endpoints. The secondary objective was to understand the relative efficacy of INT-767 to and mechanistic differences from OCA. This objective was achieved by comparing drug distribution and gene expression profiles in the liver and ileum.

Research methods

Therapeutic effects in NASH were measured using blinded qualitative (HE stained sections) and quantitative (%FA of IHC-stained sections) methods. The inclusion of a biopsy at both baseline and endpoint is unique and enabled a within-subjects, repeated-measures study design. Most studies do not include a biopsy and rely on endpoint measurements only. Morphometric assessments were also performed using label-free second harmonic generation imaging (for fibrosis) and two-photon emission (for steatosis) which are novel in NASH. The rigor of measuring the same samples using multiple histological techniques also allows the reader to consider how well these methods correlate with one another. mRNA levels of FXR regulated candidate genes were measured using RNA sequencing. LC/MS/MS was used to determine compound levels in liver and ileum.

Research results

In an 8-wk monotherapy study, INT-767 significantly improved qualitative features of NASH as demonstrated by a blinded assessment of NAS and fibrosis stage scores. Quantitatively, INT-767 significantly improved %FA for steatosis, inflammation (assessed by galectin-3 immunohistochemistry; IHC), fibrosis (Col1a1 IHC) and key components of basement membrane formation (laminin IHC). In a 16-wk comparative treatment study, NASH mice treated with INT-767 (3 and 10 mg/kg) exerted greater therapeutic potency and efficacy than OCA (10 and 30 mg/kg). Mechanistically, both OCA and INT-767 accumulate to a similar extent within the liver and ileum. INT-767 drives hepatic, but not ileal, FXR gene expression profiles more strongly than OCA, implying that the liver is a key site of action for INT-767.

Research conclusions

INT-767 improved key histological features of diet-induced and biopsy-confirmed NASH across studies using multiple methods and was shown to be more potent and efficacious than OCA. Novel insights from morphometric analyses include: (1) not only does INT-767 improve fibrosis %FA, but also the intensity of the collagen fiber signal consistent with reducing fiber density; and (2) in addition to reducing steatosis %FA, INT-767 induced a clear shift to reduce vesicular lipid droplet size believed to be more a healthful form of steatosis. Together, these preclinical findings confirm durable histological benefits with INT-767 dosing and suggest that INT-767 may exert greater efficacy than OCA.

Research perspectives

The present studies confirm and extend upon the extant literature validating FXR as a pharmacological target for NASH. Future research should consider (1) the mechanistic contribution of TGR5 to the *in vivo* effects of INT-767, and (2) the necessity and sufficiency of activating hepatic *vs* ileal FXR when targeting NASH, as INT-767 was more efficacious than OCA yet elicited only minimal ileal FXR activation. Finally, other models of diet- or toxin-induced NASH should consider incorporating a baseline biopsy to exclude mice that did not develop the desired phenotype prior to treatment initiation and gain a deeper mechanistic understanding of any pharmacologic intervention. Ongoing research continues to elucidate the role of FXR agonism on features of the basement membrane in NASH.

REFERENCES

1 **Review Team**, LaBrecque DR, Abbas Z, Anania F, Ferenci P, Khan AG, Goh KL, Hamid SS, Isakov V, Lizarzabal M, Peñaranda MM, Ramos JF, Sarin S, Stimac D, Thomson AB, Umar M, Krabshuis J, LeMair A; World Gastroenterology Organisation. World Gastroenterology Organisation global guidelines: Nonalcoholic fatty liver disease and nonalcoholic steatohepatitis. *J Clin Gastroenterol* 2014; **48**: 467-473 [PMID: 24921212]

2 **Farrell GC**, Larter CZ. Nonalcoholic fatty liver disease: from steatosis to cirrhosis. *Hepatology* 2006; **43**: S99-S112 [PMID: 16447287 DOI: 10.1002/hep.20973]

3 **Lefebvre P**, Cariou B, Lien F, Kuipers F, Staels B. Role of bile acids and bile acid receptors in metabolic regulation. *Physiol Rev* 2009; **89**: 147-191 [PMID: 19126757 DOI: 10.1152/physrev.00010.2008]

4 **Maruyama T**, Miyamoto Y, Nakamura T, Tamai Y, Okada H, Sugiyama E, Nakamura T, Itadani H, Tanaka K. Identification of membrane-type receptor for bile acids (M-BAR). *Biochem Biophys Res Commun* 2002; **298**: 714-719 [PMID: 12419312 DOI: 10.1016/S0006-291X(02)02550-0]

5 **Kawamata Y**, Fujii R, Hosoya M, Harada M, Yoshida H, Miwa

M, Fukusumi S, Habata Y, Itoh T, Shintani Y, Hinuma S, Fujisawa Y, Fujino M. A G protein-coupled receptor responsive to bile acids. *J Biol Chem* 2003; **278**: 9435-9440 [PMID: 12524422 DOI: 10.1074/jbc.M209706200]

6 **Li YT**, Swales KE, Thomas GJ, Warner TD, Bishop-Bailey D. Farnesoid x receptor ligands inhibit vascular smooth muscle cell inflammation and migration. *Arterioscler Thromb Vasc Biol* 2007; **27**: 2606-2611 [PMID: 18029909 DOI: 10.1161/ATVBAHA.107.152694]

7 **Wang YD**, Chen WD, Wang M, Yu D, Forman BM, Huang W. Farnesoid X receptor antagonizes nuclear factor kappaB in hepatic inflammatory response. *Hepatology* 2008; **48**: 1632-1643 [PMID: 18972444 DOI: 10.1002/hep.22519]

8 **Gadaleta RM**, Oldenburg B, Willemsen EC, Spit M, Murzilli S, Salvatore L, Klomp LW, Siersema PD, van Erpecum KJ, van Mil SW. Activation of bile salt nuclear receptor FXR is repressed by pro-inflammatory cytokines activating NF-κB signaling in the intestine. *Biochim Biophys Acta* 2011; **1812**: 851-858 [PMID: 21540105 DOI: 10.1016/j.bbadis.2011.04.005]

9 **Gadaleta RM**, van Erpecum KJ, Oldenburg B, Willemsen EC, Renooij W, Murzilli S, Klomp LW, Siersema PD, Schipper ME, Danese S, Penna G, Laverny G, Adorini L, Moschetta A, van Mil SW. Farnesoid X receptor activation inhibits inflammation and preserves the intestinal barrier in inflammatory bowel disease. *Gut* 2011; **60**: 463-472 [PMID: 21242261 DOI: 10.1136/gut.2010.212159]

10 **Mells JE**, Anania FA. The role of gastrointestinal hormones in hepatic lipid metabolism. *Semin Liver Dis* 2013; **33**: 343-357 [PMID: 24222092 DOI: 10.1055/s-0033-1358527]

11 **Keitel V**, Donner M, Winandy S, Kubitz R, Häussinger D. Expression and function of the bile acid receptor TGR5 in Kupffer cells. *Biochem Biophys Res Commun* 2008; **372**: 78-84 [PMID: 18468513 DOI: 10.1016/j.bbrc.2008.04.171]

12 **Baffy G**. Kupffer cells in non-alcoholic fatty liver disease: the emerging view. *J Hepatol* 2009; **51**: 212-223 [PMID: 19447517 DOI: 10.1016/j.jhep.2009.03.008]

13 **Rizzo G,** Passeri D, De Franco F, Ciaccioli G, Donadio L, Orlandi S, et al. Functional Characterization of the Semi-synthetic bile acid derivative INT-767, a dual FXR and TGR5 agonist. *Hepatology* 2010; **52**: 595A-Abstract 66.

14 **Miyazaki-Anzai S**, Masuda M, Levi M, Keenan AL, Miyazaki M. Dual activation of the bile acid nuclear receptor FXR and G-protein-coupled receptor TGR5 protects mice against atherosclerosis. *PLoS One* 2014; **9**: e108270 [PMID: 25237811 DOI: 10.1371/journal.pone.0108270]

15 **Wang X,** Herman-Edelstein M, Levi J, Gafter U, Rosenberg A, Kopp JB, et al. Dual activation of FXR and TGR5 by INT-767 mediates protection from diabetic nephropathy and retinopathy. *Am J Soc Nephrol*. 2015; **26**:169A.

16 **McMahan RH**, Wang XX, Cheng LL, Krisko T, Smith M, El Kasmi K, Pruzanski M, Adorini L, Golden-Mason L, Levi M, Rosen HR. Bile acid receptor activation modulates hepatic monocyte activity and improves nonalcoholic fatty liver disease. *J Biol Chem* 2013; **288**: 11761-11770 [PMID: 23460643 DOI: 10.1074/jbc.M112.446575]

17 **Tetri LH**, Basaranoglu M, Brunt EM, Yerian LM, Neuschwander-Tetri BA. Severe NAFLD with hepatic necroinflammatory changes in mice fed trans fats and a high-fructose corn syrup equivalent. *Am J Physiol Gastrointest Liver Physiol* 2008; **295**: G987-G995 [PMID: 18772365 DOI: 10.1152/ajpgi.90272.2008]

18 **Clapper JR**, Hendricks MD, Gu G, Wittmer C, Dolman CS, Herich J, Athanacio J, Villescaz C, Ghosh SS, Heilig JS, Lowe C, Roth JD. Diet-induced mouse model of fatty liver disease and nonalcoholic steatohepatitis reflecting clinical disease progression and methods of assessment. *Am J Physiol Gastrointest Liver Physiol* 2013; **305**: G483-G495 [PMID: 23886860 DOI: 10.1152/ajpgi.00079.2013]

19 **Kristiansen MN**, Veidal SS, Rigbolt KT, Tølbøl KS, Roth JD, Jelsing J, Vrang N, Feigh M. Obese diet-induced mouse models of nonalcoholic steatohepatitis-tracking disease by liver biopsy. *World J Hepatol* 2016; **8**: 673-684 [PMID: 27326314 DOI: 10.4254/wjh.v8.i16.673]

20 **Jouihan H**, Will S, Guionaud S, Boland ML, Oldham S, Ravn P, Celeste A, Trevaskis JL. Superior reductions in hepatic steatosis and fibrosis with co-administration of a glucagon-like peptide-1 receptor agonist and obeticholic acid in mice. *Mol Metab* 2017; **6**: 1360-1370 [PMID: 29107284 DOI: 10.1016/j.molmet.2017.09.001]

21 **Kleiner DE**, Brunt EM, Van Natta M, Behling C, Contos MJ, Cummings OW, Ferrell LD, Liu YC, Torbenson MS, Unalp-Arida A, Yeh M, McCullough AJ, Sanyal AJ; Nonalcoholic Steatohepatitis Clinical Research Network. Design and validation of a histological scoring system for nonalcoholic fatty liver disease. *Hepatology* 2005; **41**: 1313-1321 [PMID: 15915461 DOI: 10.1002/hep.20701]

22 **Liu F**, Chen L, Rao HY, Teng X, Ren YY, Lu YQ, Zhang W, Wu N, Liu FF, Wei L. Automated evaluation of liver fibrosis in thioacetamide, carbon tetrachloride, and bile duct ligation rodent models using second-harmonic generation/two-photon excited fluorescence microscopy. *Lab Invest* 2017; **97**: 84-92 [PMID: 27918557 DOI: 10.1038/labinvest.2016.128]

23 **Dobin A**, Davis CA, Schlesinger F, Drenkow J, Zaleski C, Jha S, Batut P, Chaisson M, Gingeras TR. STAR: ultrafast universal RNA-seq aligner. *Bioinformatics* 2013; **29**: 15-21 [PMID: 23104886 DOI: 10.1093/bioinformatics/bts635]

24 **Love MI**, Huber W, Anders S. Moderated estimation of fold change and dispersion for RNA-seq data with DESeq2. *Genome Biol* 2014; **15**: 550 [PMID: 25516281 DOI: 10.1186/s13059-014-0550-8]

25 **Langhi C**, Baldán Á. CIDEC/FSP27 is regulated by peroxisome proliferator-activated receptor alpha and plays a critical role in fasting- and diet-induced hepatosteatosis. *Hepatology* 2015; **61**: 1227-1238 [PMID: 25418138 DOI: 10.1002/hep.27607]

26 **Trevaskis JL**, Griffin PS, Wittmer C, Neuschwander-Tetri BA, Brunt EM, Dolman CS, Erickson MR, Napora J, Parkes DG, Roth JD. Glucagon-like peptide-1 receptor agonism improves metabolic, biochemical, and histopathological indices of nonalcoholic steatohepatitis in mice. *Am J Physiol Gastrointest Liver Physiol* 2012; **302**: G762-G772 [PMID: 22268099 DOI: 10.1152/ajpgi.00476.2011]

27 **Liang W**, Lindeman JH, Menke AL, Koonen DP, Morrison M, Havekes LM, van den Hoek AM, Kleemann R. Metabolically induced liver inflammation leads to NASH and differs from LPS- or IL-1β-induced chronic inflammation. *Lab Invest* 2014; **94**: 491-502 [PMID: 24566933 DOI: 10.1038/labinvest.2014.11]

28 **Standish RA**, Cholongitas E, Dhillon A, Burroughs AK, Dhillon AP. An appraisal of the histopathological assessment of liver fibrosis. *Gut* 2006; **55**: 569-578 [PMID: 16531536 DOI: 10.1136/gut.2005.084475]

29 **Angulo P**, Kleiner DE, Dam-Larsen S, Adams LA, Bjornsson ES, Charatcharoenwitthaya P, Mills PR, Keach JC, Lafferty HD, Stahler A, Haflidadottir S, Bendtsen F. Liver Fibrosis, but No Other Histologic Features, Is Associated With Long-term Outcomes of Patients With Nonalcoholic Fatty Liver Disease. *Gastroenterology* 2015; **149**: 389-397.e10 [PMID: 25935633 DOI: 10.1053/j.gastro.2015.04.043]

30 **Leeming DJ**, Byrjalsen I, Jiménez W, Christiansen C, Karsdal MA. Protein fingerprinting of the extracellular matrix remodelling in a rat model of liver fibrosis--a serological evaluation. *Liver Int* 2013; **33**: 439-447 [PMID: 23279004 DOI: 10.1111/liv.12044]

31 **Chalasani N**, Wilson L, Kleiner DE, Cummings OW, Brunt EM, Unalp A; NASH Clinical Research Network. Relationship of steatosis grade and zonal location to histological features of steatohepatitis in adult patients with non-alcoholic fatty liver disease. *J Hepatol* 2008; **48**: 829-834 [PMID: 18321606 DOI: 10.1016/j.jhep.2008.01.016]

32 **Rosenstengel S**, Stoeppeler S, Bahde R, Spiegel HU, Palmes D. Type of steatosis influences microcirculation and fibrogenesis in different rat strains. *J Invest Surg* 2011; **24**: 273-282 [PMID:

22047200 DOI: 10.3109/08941939.2011.586094]
33 **Xie MH**, Holcomb I, Deuel B, Dowd P, Huang A, Vagts A, Foster J, Liang J, Brush J, Gu Q, Hillan K, Goddard A, Gurney AL. FGF-19, a novel fibroblast growth factor with unique specificity for FGFR4. *Cytokine* 1999; **11**: 729-735 [PMID: 10525310 DOI: 10.1006/cyto.1999.0485]
34 **Shin DJ**, Osborne TF. FGF15/FGFR4 integrates growth factor signaling with hepatic bile acid metabolism and insulin action. *J Biol Chem* 2009; **284**: 11110-11120 [PMID: 19237543 DOI: 10.1074/jbc.M808747200]
35 **Fu T**, Kim YC, Byun S, Kim DH, Seok S, Suino-Powell K, Xu HE, Kemper B, Kemper JK. FXR Primes the Liver for Intestinal FGF15 Signaling by Transient Induction of β-Klotho. *Mol Endocrinol* 2016; **30**: 92-103 [PMID: 26505219 DOI: 10.1210/me.2015-1226]

P- Reviewer: Murotomi K, Villela-Nogueira CA **S- Editor**: Chen K
L- Editor: A **E- Editor**: Ma YJ